AFRL-RY-WP-TP-2013-0194

ULTRASENSITIVE SILICON PHOTONIC-CRYSTAL NANOBEAM ELECTRO-OPTICAL MODULATOR (PREPRINT)

Joshua Hendrickson

Optoelectronic Technology Branch
Aerospace Components & Subsystems Division

Richard Soref

University of Massachusetts

Julian Sweet and Matthew Pelton

Argonne National Laboratory

OCTOBER 2013
Interim

AIR FORCE RESEARCH LABORATORY
SENSORS DIRECTORATE
WRIGHT-PATTERSON AIR FORCE BASE, OH 45433-7320
AIR FORCE MATERIEL COMMAND
UNITED STATES AIR FORCE

REPORT DOCUMENTATION PAGE

Form Approved
OMB No. 0704-0188

1. REPORT DATE *(DD-MM-YY)*	2. REPORT TYPE	3. DATES COVERED *(From - To)*
October 2013	Journal Article Preprint	1 October 2011 – 1 October 2013

4. TITLE AND SUBTITLE
ULTRASENSITIVE SILICON PHOTONIC-CRYSTAL NANOBEAM ELECTRO-OPTICAL MODULATOR (PREPRINT)

5a. CONTRACT NUMBER
In-house

5b. GRANT NUMBER

5c. PROGRAM ELEMENT NUMBER
61102F

6. AUTHOR(S)
Joshua Hendrickson (RYDH)
Richard Soref (University of Massachusetts)
Julian Sweet and Matthew Pelton (Argonne National Laboratory)

5d. PROJECT NUMBER
3001

5e. TASK NUMBER
12

5f. WORK UNIT NUMBER
Y00W

7. PERFORMING ORGANIZATION NAME(S) AND ADDRESS(ES)
Optoelectronic Technology Branch
Aerospace Components & Subsystems Division
Air Force Research Laboratory, Sensors Directorate
Wright-Patterson Air Force Base, OH 45433-7320
Air Force Materiel Command, United States Air Force

University of Massachusetts
Argonne National Laboratory

8. PERFORMING ORGANIZATION REPORT NUMBER
AFRL-RY-WP-TP-2013-0194

9. SPONSORING/MONITORING AGENCY NAME(S) AND ADDRESS(ES)
Air Force Research Laboratory
Sensors Directorate
Wright-Patterson Air Force Base, OH 45433-7320
Air Force Materiel Command
United States Air Force

10. SPONSORING/MONITORING AGENCY ACRONYM(S)
AFRL/RYDH

11. SPONSORING/MONITORING AGENCY REPORT NUMBER(S)
AFRL-RY-WP-TP-2013-0194

12. DISTRIBUTION/AVAILABILITY STATEMENT
Approved for public release; distribution unlimited.

13. SUPPLEMENTARY NOTES
Journal article to be published in Optics Express. ©2013 OSA. The U.S. Government is joint author of the work and has the right to use, modify, reproduce, release, perform, display or disclose the work. PAO Case Number 88ABW-2013-1047, Clearance Date 5 March 2013. Report contains color.

14. ABSTRACT
Design and simulation results are presented for an ultralow switching energy, resonator based silicon-on-insulator (SOI) electro-optical modulator. The nanowire waveguide and resonator are seamlessly integrated via a high-transmission tapered 1D photonic crystal cavity waveguide structure.

15. SUBJECT TERMS
electro-optical, silicon-on-insulator, modulator, photonic-crystal

16. SECURITY CLASSIFICATION OF:			17. LIMITATION OF ABSTRACT:	18. NUMBER OF PAGES	19a. NAME OF RESPONSIBLE PERSON (Monitor)
a. REPORT	b. ABSTRACT	c. THIS PAGE			Joshua Hendrickson
Unclassified	Unclassified	Unclassified	SAR	12	19b. TELEPHONE NUMBER *(Include Area Code)* N/A

Ultrasensitive silicon photonic-crystal nanobeam electro-optical modulator

Joshua Hendrickson,[1,*] Richard Soref,[2] Julian Sweet,[1,3] Matthew Pelton[3]

[1]*Air Force Research Laboratory, Sensors Directorate, Wright-Patterson Air Force Base, Ohio, 45433, USA*
[2]*Department of Physics & Engineering Program, University of Massachusetts at Boston, Boston, MA 02125 USA*
[3]*Center for Nanoscale Materials, Argonne National Laboratory, Argonne, Illinois 60439, USA*
[*]*joshua.hendrickson@wpafb.af.mil*

Abstract: Design and simulation results are presented for an ultralow switching energy, resonator based silicon-on-insulator (SOI) electro-optical modulator. The nanowire waveguide and resonator are seamlessly integrated via a high-transmission tapered 1D photonic crystal cavity waveguide structure. A lateral p-n junction of modulation length ~λ is used to alter the index of refraction through fast carrier depletion. Differential signaling of the device with ΔV ~1Volt allows for a 3dB extinction ratio at telecom wavelengths with an energy cost as low as 19attojoules/bit.

OCIS codes: (230.5298) Photonic crystals; (250.7360) Waveguide modulators; (230.2090) Electro-optical devices.

References and links

1. Q. Quan and M. Loncar, "Deterministic design of wavelength scale, ultra-high Q photonic crystal nanobeam cavities," Opt. Express **19**, 18529-18542 (2011).
2. B. Qi, P. Yu, Y. Li, X. Jiang, "Analysis of electrooptic modulator with 1-D slotted photonic crystal nanobeam cavity," IEEE Photonics Technology Letters **23**, 992-994 (2011).
3. V. J. Sorger, "λ-size silicon-based modulator," invited paper 8629-23, SPIE Proceedings vol. 8629, Silicon Photonics VIII, SPIE Photonics West, San Francisco, 5 Feb 2013.
4. Q. Quan, P. B. Deotare, and M. Loncar, "Photonic crystal nanobeam cavity strongly coupled to the feeding waveguide," Appl. Phys. Lett. **96**, 203102 (2010).
5. N.-N. Feng, S. Liao, D. Feng, P. Dong, D. Zheng, H. Liang, R. Shafiiha, G. Li, J. E. Cunningham, A. V. Krishnamoorthy, and M. Asghari, "High speed carrier-depletion modulators with 1.4V-cm $V_{\pi}L$ integrated on 0.25μm silicon-on-insulator waveguides," Opt. Express **18**, 7994-7999 (2010).
6. M. Nedeljkovic,, R. A. Soref, and G. Z. Mashanovich, "Free-carrier electrorefraction and electroabsorption modulation predictions for silicon over the 1-14 μm infrared wavelength range," IEEE Photonics Journal 3(6), 1171-1180 (2011).
7. M. Nedeljkovic,, R. A. Soref, and G. Z. Mashanovich, "Free-carrier electro-absorption and electro-refraction modulation in group IV materials at mid-infrared wavelengths," SPIE Photonics West, paper 8266-31, San Jose, CA (25 Jan 2012).
8. D. A. B. Miller, "Energy Consumption in optical modulators for interconnects," Opt. Express 20, A293-A308 (2012).
9. H-C. Liu and A. Yariv, "Designing coupled-resonator optical waveguides based on high-Q tapered grating-defect resonators," Opt. Express **20**, 9249-9263 (2012).
10. C. Qiu, J. Chen, and Q. Xu, "Ultraprecise measurement of resonance shift for sensing applications," Opt. Lett. **37**, 5012-5014 (2012).
11. R. A. Soref, J. Guo, and G. Sun, "Low-energy MOS depletion modulators in silicon-on-insulator micro-donut resonators coupled to bus waveguides," Opt. Express **19**, 18122-18134 (2011).
12. W. S. Fegadolli, J. E. B. Oliveira, V. R. Almeida, and A. Scherer, "Compact and low power consumption tunable photonic crystal nanobeam cavity," **21**, 3861-3871 (2013).
13. W. A. Zortman, A. L. Lentine, D. C. Trotter, and M. R. Watts, "Vertical junction silicon microdisk modulators and switches," Opt. Express **19**, 21989-22003 (2011).
14. W. A. Zortman, A. L. Lentine, D. C. Trotter, and M. R. Watts, "Low-voltage differentially-signaled modulators," Opt. Express **19**, 26017-26026 (2011).

1. Introduction

Electro-optical modulation in silicon nanobeams produced by the depletion or injection of electrons and holes is investigated in this paper. Silicon nanobeam (NB) components are a silicon-on-insulator (SOI) technology. The NB is a single-mode Si strip channel waveguide or Si "photonic nanowire" that includes a resonant cavity at a telecom wavelength in the present case. The resonance is created by a 1D photonic crystal (PhC) lattice which is a series of cylindrical air holes etched into the Si down to the buried oxide interface. A high transmission, high quality factor waveguide-cavity system can be made from a series of quadratically tapered holes with a zero-length cavity region in the middle. The series of holes on each side of the cavity can be thought of as a Bragg mirror.

Prior examples of resonant nanowire electro-optical (EO) modulators consist mainly of a bus waveguide that is evanescently side-coupled through an air gap to a micro-ring, micro-disk or micro-donut, i.e., the resonator is a separate entity from the nanowire. In contrast, our device has the resonator and optical transmission waveguide seamlessly combined in one wire resulting in a much smaller footprint. Owing to these device area considerations, the NB EO modulator offers the possibility of a significantly lower switching energy than the disk/ring approach.

Previous EO modulator implementations employ carrier injection in a Si NB[1], whereas this paper investigates the use of carrier depletion.

Another approach outlined by Qi *et al* [2] studies a nanoscale slot that is etched into the midline of a high quality factor (Q) nanohole array allowing for the introduction of an EO polymer. With doped silicon contact regions straddling that slot, it is proposed that applied voltage perturbing the polymer will shift the nanobeam resonance. We agree that the slot NB resonator offers the smallest possible cavity volume and switching energy. The purpose of our proposed project is to estimate what can be done without a slot using the free-carrier plasma dispersion effect in its "fastest embodiment"—which is the lateral p-n junction electron-hole depleter. In many ways, this specific depletion architecture emulates the aforementioned slot design as the vertical depletion layer closely resembles a slot in both cross-sectional dimensions and active length. Therefore, looking at the slot and the depleter collectively, we believe that these Si EO NB structures offer the fastest and lowest-energy modulation in silicon photonics (not considering here the sub-wavelength modulator capabilities of plasmonics and plasmon-photonics [3]). Also, consider the disadvantage of the extrinsic nature of the EO polymer, as it is a guest inserted inside of the silicon host. On the other hand, the p-n depleter is intrinsic, meaning that the active material is seamlessly and monolithically integrated into the NB. This results in a device that is easier to manufacture and is more CMOS-compatible.

2. Device Design

Our design consists of a 1D silicon-on-insulator (SOI) photonic crystal nanobeam cavity strongly coupled to a feeding waveguide. Such devices offer high optical transmission as well as a high quality factor and a small mode volume. The fundamental mode optical transmission consists of a Lorentzian peak situated midway in the PhC's low background forbidden gap transmission spectrum.

Several design algorithms have recently been proposed; in our example we follow that outlined by the Loncar group [4] where the photonic crystal hole size (or equivalently the fill factor) is quadratically tapered down from the center of a zero length cavity region to either edge of the photonic crystal. This creates a linear change in the photonic crystal mirror strength, allowing for efficient coupling between the waveguide structure and the photonic crystal structure.

The device consists of a 500nm wide by 220nm high silicon strip waveguide on top of a silicon dioxide layer. While performance of 1D photonic crystal nanobeam structures can be increased by creating suspended structures through undercutting of the buried oxide layer beneath the device, we have chosen to leave our device on the substrate for maximum robustness. The oxide is assumed to be optically thick. The number of mirror pairs in the TE_0-mode photonic crystal was chosen to be 12 (a total array of 24) which results in a quality factor slightly below 10^4. We found this to be a fair tradeoff between the resonance linewidth and the cavity lifetime which are inversely proportional quantities. If the quality factor is too high, the speed of the device is compromised. However, if the quality factor is too low then very large modulation shifts of the wavelength are required due to the large bandwidth of low Q resonators. A periodicity of 350nm was selected in order to get device operation in the telecom-friendly 1500nm range. We note that one could easily adjust this parameter in order to tweak the actual wavelength of operation to any other desired value, such as 1550nm. The fill factor of the center two holes was chosen to be 0.2 and was quadratically tapered down to 0.1 at the outer two holes. This results in a quadratic tapering of the hole radii from roughly 125nm to 88nm. For electrical contact and for defining the p-n junction, initially undoped 50nm-thick silicon "wings" extending the entire length of the photonic crystal device were placed on either side of the nanobeam. The Si wings-on-oxide integrate seamlessly with the nanowire and a cross-section view in the wing region shows the geometry of a rib waveguide. Voltage contacts for electro-optic modulation are made in doped wing areas.

P-type and n-type doping of the respective left and right wings is then performed as shown in the NB perspective view of Fig. 1(a), orange for p and dark green for n—with doping length centered on the cavity. The next design consideration consisted of choosing the appropriate hole and carrier doping concentrations and the exact lateral position of the abrupt p-n junction [5]. While higher doping concentrations can lead to larger changes in the refractive index they also result in higher levels of loss due to free carrier absorption. A compromise of these two parameters led us to choose a p-type doping concentration of $5x10^{17}$ cm^{-3} and an n-type doping concentration of $1x10^{18}$ cm^{-3}, p-type being slightly less since holes have a greater effect on the optical index of refraction. Both the nanobeam and the "wings" are doped by the same amount and to the same length, L_m, which is the modulator's interaction length. Note that the 24-hole on-axis length of the lateral wings L_w overlapping the array is always held constant and that only a fraction L_m/L_w of the wing is doped. The reason for this is that wings with a length shorter than that of the photonic crystal structure resulted in significant transmission loss of the device. As illustrated in the cross-section cavity view of Fig. 1(b), the width of the p-type doped region in the nanobeam was set to 285nm and the width of the n-type doped region was set to 215nm. The position of the p-n junction is, therefore, not actually centered in the nanobeam but is offset by 35nm. Our simulation results, which follow, show that this is an optimized junction location for our device. A top view of the EO NB is shown in Fig. 2.

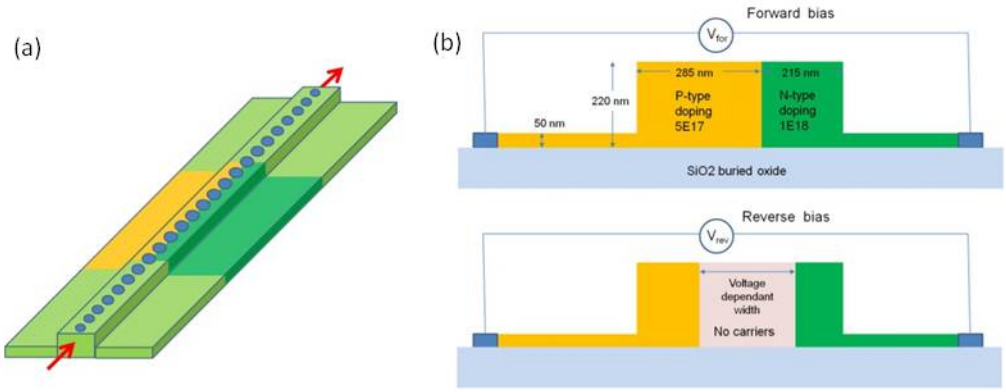

Fig. 1: (a) schematic view of device and (b) cross sectional views of the device for forward and reverse bias taken through the center of the photonic crystal cavity region

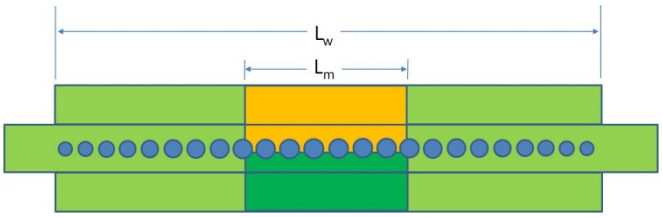

Fig. 2: Top down view of device

3. Simulations

Simulations were carried out using a commercially available finite difference time domain software package (Lumerical FDTD). A transverse electric waveguide mode was input into one end of the structure and the intensity transmission through the device was calculated at the other end. Within the photonic crystal structure area, a mesh size of 10nm along the length and height and 5nm across the width was used. The simulation time was set to 80ps. For the doped regions a complex refractive index of n=3.474148 and k= 0.000112 was used for the n-type regions and n=3.473960 and k=0.000031 for the p-type regions [6,7]. In the depleted regions a value of n=3.475 and k=0 was used.

With zero voltage applied across the p-n junction, an intrinsic depletion region 60nm wide is formed. The built-in voltage, V_o, of this p-n device is calculated to be 935mV. Applying a forward bias of 0.935V (bucking out V_o) injects enough carriers to completely eliminate this depletion region. Zero depletion width is then used as our standard and compared to various finite depletion layer widths, equivalent to various applied reverse biases across the p-n junction. Table 1 lists the voltage values used and corresponding depletion widths. Non-intuitive values of voltage were used in order to generate depletion widths that are odd multiples of 10, thereby ensuring that the edges of the depletion width are located exactly on lines of the simulation mesh grid.

Table 1. Width of the depletion region as a function of applied voltage

Bias Voltage(V)	Depletion width (nm)
0.935	0
-0.315	70
-1.14	90
-2.16	110

In order to determine the optimal p-n junction location, a serious of simulations were performed. Using an arbitrary modulation length of 2 microns, the resonance shift between +0.935V and -1.14V was determined for six different p-n junction locations. Fig. 3(a) shows the transmission spectra for each simulation and Fig. 3(b) shows a plot of wavelength shift as a function of junction location, given as a ratio of the p-type doped region width to the n-type doped region width. One can easily see that the greatest shift occurs when the p-type region is 285nm and the n-type region is 215nm which gives a 35nm p-n junction offset from center.

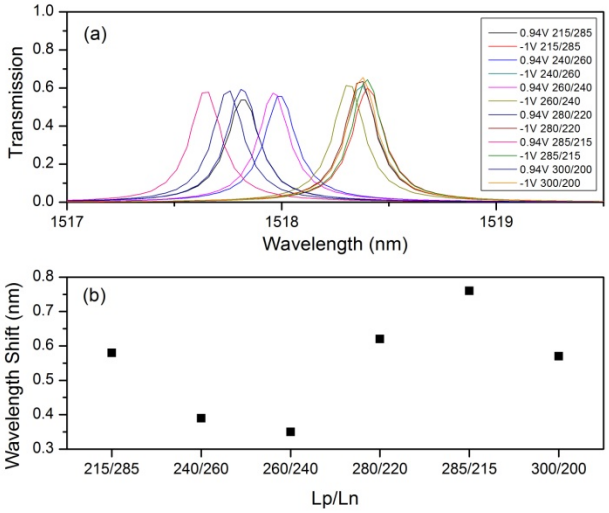

Fig. 3: 2μm modulation length (a) transmission spectra at 0.935v and -1.14V for various pn junction offsets and (b) modulation shift as a function of p-n junction offset

After determining the optimal p-n junction offset, a number of simulations were carried out in order to characterize the functionality of our device. Transmission spectra were obtained for six different modulation lengths: 0.1μm, 0.2μm, 0.5μm, 1μm, 2μm, and 5μm. Each of these modulation lengths was simulated for our four different bias voltages: +0.935V, -0.315V, -1.14V, and -2.16V. All twenty four transmission spectra are shown in Fig. 4.

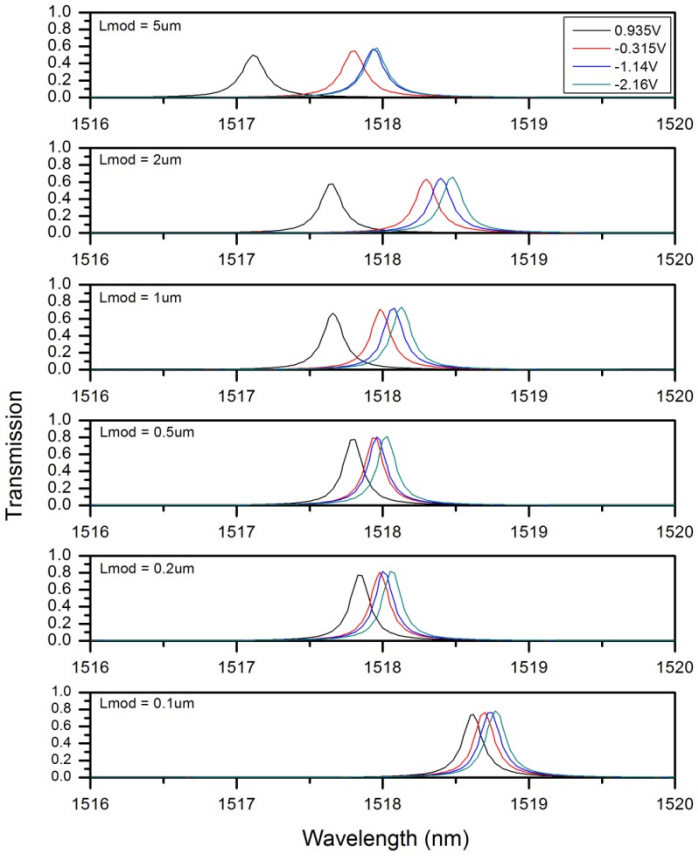

Fig. 4: Transmission spectra as a function of applied voltage and modulation length

4. Results

The most important aspects are our device, namely the extinction ratio ER, the modulation shift $\Delta\lambda$ of the resonance wavelength λ_o, the quality factor Q, and the peak optical power transmission value T are all shown in Fig. 5 as a function of modulation length L_m. For short modulation lengths the transmission, Fig. 5(a), hovers up around 80%, decreasing down to 50-60% for the longest modulation length of 5μm. This is to be expected as longer modulation lengths result in increased free carrier absorption. Also, as expected, narrower depletion width results in a slightly lower transmission value when compared to wider depletion widths which is simply a result of the decreased number of free carriers in the depletion region. This effect is also mirrored in the quality factor values shown in Fig. 5(b), with Q's in the 10k range for 0.1-0.5 μm modulation lengths, decreasing down to the 8k range for 5μm modulation length. Fig. 5(c) shows the wavelength shift and Fig. 5(d) the extinction ratio ER as referenced from the 0.935 forward bias (i.e. zero depletion width) resonance position; ER = $T(\lambda_o,V_o)/T(\lambda_o,V_R)$. The wavelength shift ranges from a minimum of 0.08nm for a 0.935V to -0.314V voltage swing at 0.1 μm modulation length to a maximum of 0.85nm for a 0.935V to -2.16V voltage swing at 5 μm modulation length. Most importantly, the extinction ratio did not fall below 3dB for any of our simulation modulation lengths and/or voltage swings.

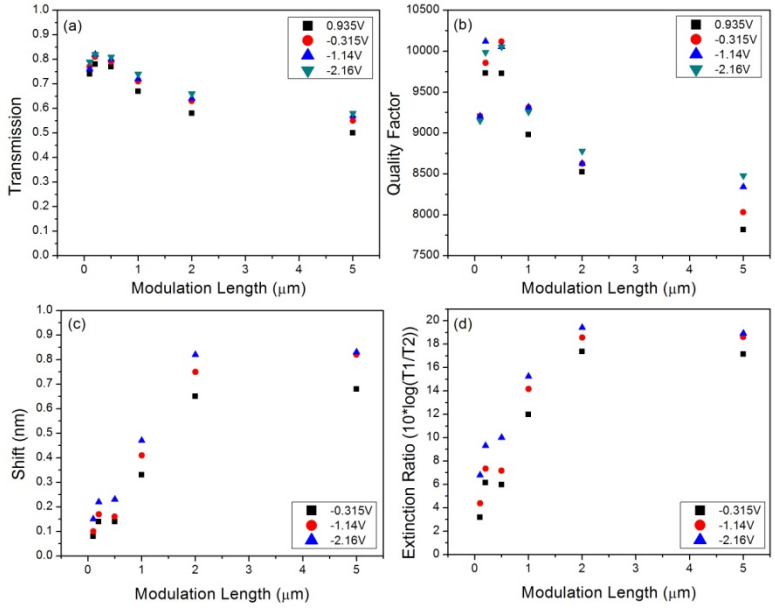

Fig. 5: (a) transmission, (b) quality factor, (c) shift, and (d) extinction ratio as a function of modulation length.

In order to calculate an estimate for the required switching energies for our different device parameters, one must first determine the junction capacitance of the device. For reverse bias (and zero bias) conditions, we used the following standard formula for junction capacitance:

$$C_{rev} = A\sqrt{\left(\frac{\varepsilon_s q}{2}\right)\left(\frac{N_d N_a}{N_d + N_a}\right)\left(\frac{1}{V_o - V_R}\right)} \tag{1}$$

where A is the junction area (modulation length x nanobeam height), ε_s is the permittivity of silicon, N_d and N_a are the p-type and n-type doping concentrations, V_o is the built in potential, and V_R is the applied reverse bias. For the full forward bias situation, 0.935V, we used the standard rule of thumb:

$$C_{for} \approx 2C_0 \tag{2}$$

where C_{for} is the forward bias junction capacitance and C_0 is the junction capacitance corresponding to the built in potential. The switching energy,E_s, is then calculated [8] as

$$E_s = \frac{1}{2}\left(C_{for}V_o^{\,2} + C_{rev}V_R^{\,2}\right) \tag{3}$$

In a typical digital logic scheme, one can think of the switching energy as the energy required in order to flip a bit, therefore, the units of E_s can be expressed as Joules per bit flip. Since the probability of a bit flip is 50%, the average energy per bit E_b is ½ that of the switching energy,

$$E_b = \frac{1}{2}E_s \tag{4}$$

Table 2 lists the energy per bit required for various modulation lengths when switching from full forward bias of 0.935V to a reverse bias of -0.315V, -1.14V, and -2.16V. For a 0.1μm modulation length and a 0.935 to -0.315 modulation-voltage swing, where $C_{0.935}$ = 81 aF and $C_{-0.315}$ = 35 aF is calculated, the E_b required for 3dB of extinction is only 19 attojoules per bit. We would like to note that our estimates for capacitance and, hence, energy, do not take into account the air holes in the photonic crystal structure which we expect would only slightly modify our results. Furthermore, the 0.1μm modulation length does not extend into the holes of the photonic crystal since the edge to edge spacing of the center two holes is also 0.1μm.

Table 2: Energy per bit E_b required to switch from 0.935V to various reverse bias voltages for various modulation lengths.

L_m (μm)	Energy/bit for -0.315V switching (fJ)	Energy/bit for -1.14V switching (fJ)	Energy/bit for -2.16V switching (fJ)
0.1	0.019	0.027	0.044
0.2	0.037	0.053	0.088
0.5	0.093	0.133	0.219
1	0.186	0.266	0.438
2	0.372	0.532	0.876
5	0.931	1.330	2.189

5. Discussion

Most of the published implemenations of 1550nm SOI electro-optical modulators consist of a Si strip waveguide side coupled to a Si micro-ring or micro-disk resonator containing a circumferential p-n junction for carrier depletion in the cavity. By comparison, our Si NB EO modulator has a smaller footprint because it foregoes the micro-ring or disk. In addition, the NB modulator has a smaller mode volume within the active region than the ring modulator, allowing lower switching energy in the NB. The resonance characteristics are also different because the NB, with its 1D PhC cavity, possesses one or two high transmission peaks within the low transmission gap of the photonic crystal, while the micro-disk offers a long periodic series of resonances. In addition to coupling several NBs cavities serially along one wire [9], it is feasible to arrange an evanescent wave side coupling of a NB to one or more parallel NBs or to one or more non-resonant SOI channel waveguides. We expect to study EO versions of those NB directional couplers in the future.

Also consider that germanium becomes transparent for $\lambda > 1.8$ μm and possesses a free-carrier depletion effect much stronger than that of silicon. Therefore, a Ge nanobeam EO modulator corresponding to the present device design is anticipated to be even more sensitive than a Si device.

The Si NB can also serve as a refractometer if the Si NB resonance wavelength λ_o is chosen to correspond to the fundamental absorption line of a target molecular species and if this analyte is infused into the pores of the Si modulator, serving as a new upper cladding material instead of air. Then the complex cladding index of the NB will change substantially in the presence of the analyte, thereby shifting the NB resonance. Since the NB is EO, it is possible to "dither" the cavity resonance at audio frequencies, allowing for an extremely precise measurement of λ_o and its shift. This measurement method has been described by Qiu *et al* [10] who show that the resonance of the refractometer can be measured to within 0.16 pm, thus enhancing the refractometer sensitivity.

As a final comment, we note that this NB modulator is highly versatile because it can be actuated by several available physical mechanisms for actively shifting λ_o of the Si NB. These are: a p-i-n or p-n junction for electron and hole depletion or injection, an MOS high-K gate on the NB for carrier depletion or accumulation [11], a micro-heater-induced thermo-optic effect [12], the Franz-Keldysh field effect operative around 1100 nm, and two nonlinear optical effects; (1) generation of e-h pairs in the resonator due to an above gap light beam incident on the Si, (2) an intensity dependent refractive index n_2 of the cavity induced by strong optical pumping of the third-order nonlinear Si. We have selected p-n depletion as the most practical technique. Furthermore, we had a choice of depleting either a lateral p-n junction or a vertical p-n junction. The vertical junction is thought to be almost twice as efficient as the horizontal junction [13], although an air bridge contact may be required in the vertical case. We chose to use the lateral junction which has been applied quite successfully in the Si modulator literature [5]. The vertical junction NB awaits future exploration.

6. Conclusion

We have simulated an SOI thick-oxide lateral p-n junction modulator compatible with the low-voltage differential signaling described by Zortman et al [14], By examining the case of 935mV forward bias combined with 315mV reverse bias (asymmetric signaling), we achieved a 6dB extinction ratio (L_m = 0.2 μm) at the 1D PhC cavity resonance λ_o ~1518 nm. In the 500nm x 220nm TE_0-mode Si nanobeam, a point-defect resonator was not used, and instead the cavity consisted of a zero-length defect midway in an array of 24 cylindrical air holes whose diameter was quadratically tapered in and out from 250 to 176 nm, The Si strip waveguide became a fixed-length rib waveguide over the L_w = 8.2 μm PhC array length where 50nm high Si lateral wings, initially undoped, extended out from both sides of the NB. To create a horizontal abrupt p-n junction in the NB, and to provide external electrical contacts for bias voltage, the left and right portions of the NB were locally doped over the central region of the hole array, as were the left and right wings. The p type doping was $5x10^{17}$ cm^{-3} and the n type doping was $1x10^{18}$ cm^{-3}. Simulation tests showed that a 35 nm offset of the junction from the NB center (p width=285nm, n width=215nm) produced the best modulation.

For a 24-hole device simulated using Lumerical FDTD, we estimate the following performance features: (1) the information bandwidth is approximately 20 GHz as calculated from the "worst case" cavity linewidth of 152 pm, (2) the active modulator length of 0.1 to 1 μm of this "all-dielectric Si wire" is truly wavelength-scale and ranges from 0.066λ to 0.66λ, (3) the λ_o shift per unit applied-voltage swing per unit length $\Delta\lambda/\Delta V$ L_m is a figure of merit (FOM) and this FOM is maximum at ~ 0.6nm/Vμm when $\Delta V=V_o-V_R$ ~ 1V and L_m ~ 0.2 μm, (4) the infrared transmission at λ_o is ~ 80% for optimum cases, meaning an insertion loss of ~1dB, and (5) the minimum forward/reverse switching energy for 3dB of ER is extremely low; for example E_b = 19 attojoules per bit at V_R = 315mV and L_m = 0.1 μm. These specifications, taken as a whole, indicate very high modulation sensitivity, a performance that exceeds the performance reported for Si micro ring and disk modulators.

The most practical range of NB operation is for modulation lengths of 0.1 to 0.5 μm, with ΔV~1V. The ER in Fig. 5(d) depends more strongly upon L_m than upon V_R. Consequently, we infer that V_R could be reduced to very low values while preserving high performance. For example, a reverse signaling voltage of only 100 mV is estimated to give ER > 3dB when L_m~ 0.2 μm. As we have found that E_b is roughly proportional to L_m, ΔV, Δλ and ER, we can use these guidelines to minimize E_b while keeping L_m < 0.5μm for high T. Therefore, even for an ER of 6dB, there are many choices of L_m and ΔV that will give a switching energy of less than 100 aJ/bit.

Acknowledgements

JH and JS would like to acknowledge support from the Air Force Office of Scientific Research (Program Manager Dr. Gernot Pomrenke) under contract number 12RY05COR. RS appreciates AFOSR support under grant FA9550-10-1-0417.